

Cavendish-HEP-99/11
 DAMTP-1999-148
 hep-ph/0001038

Gribov's Equation for the Green Function of Light Quarks*

Carlo Ewerz

*Cavendish Laboratory, Cambridge University
 Madingley Road, Cambridge CB3 0HE, UK*

and

*DAMTP, Centre for Mathematical Sciences, Cambridge University
 Wilberforce Road, Cambridge CB3 0WA, UK*

email: *carlo@hep.phy.cam.ac.uk*

Abstract

Gribov's scenario of supercritical charges in QCD is investigated. We perform a numerical study of the corresponding equation for the Green function of light quarks. This is done in an approximation which neglects all pion contributions. Different types of solutions in the Euclidean region are discussed and the mass function of the quark is calculated. The solutions of the equation are shown to have a qualitatively different behaviour if the strong coupling constant α_s exceeds a critical value $\alpha_c = 0.43$ in the infrared region. Chiral symmetry breaking is found to occur at supercritical coupling. The analytic structure of the solutions is investigated. Earlier results obtained by Gribov are confirmed and extended.

*Work supported in part by the EU Fourth Framework Programme 'Training and Mobility of Researchers', Network 'Quantum Chromodynamics and the Deep Structure of Elementary Particles', contract FMRX-CT98-0194 (DG 12 - MIHT).

1 Introduction

The breaking of chiral symmetry and the confinement of quarks and gluons are two of the most important properties of QCD. The details of the mechanism leading to confinement are still largely unknown, and the understanding of non-perturbative dynamics in QCD in general is still rather poor. A new picture of the confinement mechanism and of chiral symmetry breaking was developed by V. N. Gribov [1]–[4]. It is based on the phenomenon of supercritical charges which can occur in QCD due to the existence of very light quarks. Its consequence is a dramatic change in the vacuum structure of the light quarks compared to the usual perturbative picture at small coupling.

The phenomenon of supercritical charges is well-known in QED (for an extensive review see [5]). The energy of the bound-state levels in the field of an isolated heavy nucleus decreases if the charge Z of the nucleus is increased. When the charge exceeds a critical value¹ of $Z_{cr} = 137$, the lowest bound-state level dives into the Dirac sea, i. e. sinks below $-m_e$. As a consequence an electron from the (filled) continuum undergoes a transition into this level, and a positron is emitted. The electron is said to ‘fall onto the center’. In this situation the simple quantum mechanical picture breaks down, and the emerging bound state is in fact a collective state with a high probability to find an electron very close to the nucleus. This mechanism is called supercritical binding. The condition for its occurrence is that the Compton wavelength $1/m$ of the electron is much larger than the radius of the heavy charge.

Gribov’s confinement scenario is based on the idea that a similar phenomenon occurs in QCD due to the existence of very light (almost massless) quarks. The crucial point is that in this scenario already the color charge of a single quark is supercritical. Since this applies also to the light quarks themselves the situation is more involved than in QED. We will give only a condensed description of the resulting scenario here. More detailed accounts have been given in [2, 4, 6, 7]. In order to get an understanding of the underlying physical picture we again use the quantum mechanical description, having in mind that the quantitative analysis should be based on the full underlying quantum field theory.

The confinement of heavy quarks in Gribov’s scenario is very similar to the supercritical binding in QED. Due to its supercritical charge the heavy quark captures a light antiquark from the vacuum, thus decaying into a supercritical heavy–light bound state. At the same time a light quark is created. This light quark decays again, as we will discuss now.

In order to understand the confinement of light quarks, we first consider a bound state of a light quark and a light antiquark. If the coupling constant is small this is just a normal bound state like positronium in which the quarks have positive kinetic energy. If we now increase the coupling the binding energy will also increase. The total energy of this state will thus decrease. But if the coupling is further increased — and becomes supercritical — a situation is possible in which the total energy of the bound state becomes negative. In order to have a stable vacuum, however, the existence of negative energy particles has to be avoided. Consequently, the corresponding quark states in the supercritical bound states have to be filled in the vacuum. Therefore there are filled quark states with positive kinetic energy in addition to the usual filled states in

¹This number holds for a point-like nucleus, for an extended charge it is around $Z_{cr} \sim 165$.

the Dirac sea (see² Fig. 1). The scale μ_F separating filled and empty states of positive

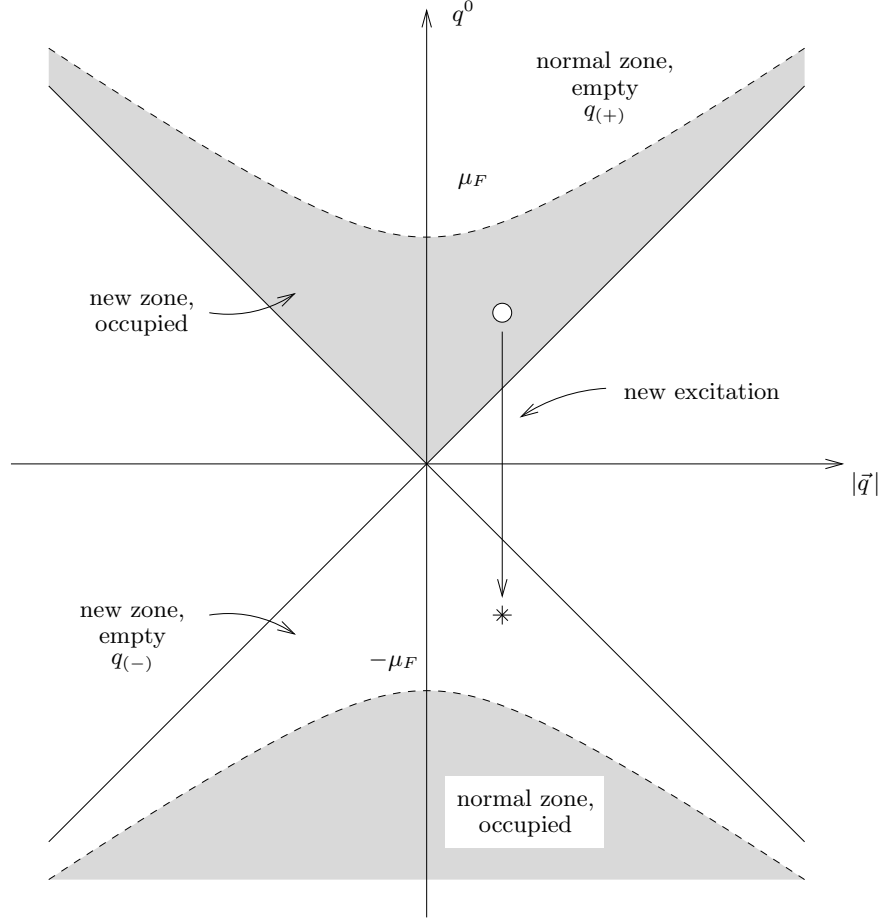


Figure 1: Vacuum of light quarks in Gribov's scenario. q^0 and \vec{q} denote the (kinetic) energy and three-momentum, respectively.

kinetic energy resembles the Fermi surface in solid state physics. The existence of the additional states in the vacuum of light quarks implies also the existence of additional excitations of this vacuum which have quite unusual properties. The $q\bar{q}$ pair of such an excitation forms a supercritical bound state in which the quark and antiquark both have negative kinetic energy. They are interacting repulsively, and the supercritical bound state has positive total energy. The 'binding force' leading to this unusual meson³ is the Pauli exclusion principle. The quark and antiquark are bound in this meson because all other energetically possible states in the vacuum are already filled.

Having discussed the emergence of the novel meson states, we can now understand the confinement of light quarks. According to Gribov it is caused by the continuous decay of the light quark. Any quark (with positive or negative kinetic energy, $q_{(+)}$ or $q_{(-)}$) decays into a supercritical bound state M and a quark $q_{(-)}$ of negative kinetic

²In this figure only the energy of the quark is shown. One has to keep in mind that some of the states shown here exist only within supercritical bound states with an antiquark as described above.

³Some possible properties of these novel mesons have been discussed in [8, 9].

energy,

$$q_{(\pm)} \rightarrow M + q_{(-)} . \quad (1)$$

In this sense the quark exists only as a resonance and cannot be observed as a free particle.

Since the existence of the novel meson states is due to the Pauli principle it is immediately clear that the above confinement mechanism works only for quarks but not for gluons. But the confinement of gluons could possibly be a ‘second order effect’ in Gribov’s scenario, namely due to their coupling to light quarks which subsequently decay as described above.

It is obviously desirable to find a quantitative description for this interesting physical picture of supercritical color charges. The confinement of quarks and gluons should be encoded in the singularities of the respective Green functions. Therefore the Green function of the quark is a suitable object to study in this context. In [2, 3] Gribov derived an equation for the retarded Green function of light quarks. It takes into account especially the dynamics of the infrared region but also reproduces asymptotic freedom at large momenta. Chiral symmetry breaking has been found to occur when the strong coupling constant exceeds a critical value, leading to the emergence of Goldstone boson (pions). It has been argued in [3] that the nature of these Goldstone bosons is such that they should in fact be regarded as elementary objects. Corrections to the Green function caused by these Goldstone bosons are expected [4] to lead a Green function of light quark which exhibits confinement, whereas the equation without these corrections is not expected to imply confinement [2, 3]. Unfortunately, the paper [4] remained unfinished, and a full study of the analytic properties of the Green function and their consequences still remains to be done. Especially, it will be important to see how and to what extent the — though somewhat simplified — physical picture described above can be derived from the analytic properties of the resulting Green function.

Gribov’s equations for the Green function of light quarks (with or without pion corrections) are non-linear differential equations. So far the studies of these equations [2, 3, 4] have been performed only by means of asymptotic expansions. It is the purpose of the present paper to perform a complete numerical study of the equation without pion corrections. This allows us to study the breaking of chiral symmetry also quantitatively and in more detail. We also investigate the analytic structure of the Green function resulting from Gribov’s equation.

It turns out that in Gribov’s equation the critical value of the strong coupling constant is surprisingly low, $\alpha_c = 0.43$. In the derivation of the equation it is assumed that the coupling constant does not become very much larger than this critical value. To some extent Gribov’s approach can thus be considered as a semi-perturbative approach to confinement. This picture might also explain why we observe an essentially smooth behaviour of non-perturbative effects in the transition from the parton level to the hadron level. Typical multiplicities at the parton level, for example, are in surprising correspondence to those observed at the hadron level (for a more detailed discussion of this and similar observations see [10]). The idea of an infrared finite coupling has also been widely discussed in the context of power corrections and the dispersive approach to renormalons in QCD [11, 12], see also [13] and references therein. In that approach, it appears consistent to define an effective running coupling down to very low momentum

scales, in the sense that its first moments have a universal meaning. The values of the coupling found in the corresponding experimental analyses are in fact bigger than the critical value in Gribov's equation.

The equation can be derived from the Dyson–Schwinger equation for the Green function of the quark in Feynman gauge. The approximations made in the derivation are motivated by the underlying physical picture, especially concerning the behaviour of the strong coupling constant. This method can therefore also be viewed as an unconventional approach to the difficult problem of solving the Dyson–Schwinger equations in QCD (for a review see [14]). The approximations usually made in solving the Dyson–Schwinger equations are intrinsically difficult to control. Comparisons with results obtained in Gribov's approach will therefore be potentially very useful.

The paper is organized as follows. In section 2 we outline the main steps leading to the equation for the Green function of light quarks and describe some of its most important properties. In section 3 a suitable parametrization of the Green function is given. The asymptotic behaviour of the equation for small and large momenta is discussed and the critical value of the strong coupling constant is derived. Section 4 deals with the Euclidean region of space-like momenta. In section 4.1 the solutions are shown to exhibit asymptotic freedom at large space-like momenta. Section 4.2 provides models for the running coupling at small (space-like) momenta which are needed for the numerical analysis of the equation. The possible types of solutions in the Euclidean region are classified in section 4.3. The characteristic change in the solutions at supercritical coupling is discussed. Section 5 deals with the behaviour of the dynamical mass function of the quark in the Euclidean region. Phase transitions are found to occur for supercritical coupling and lead to chiral symmetry breaking. We study how this effect depends on the models used for the running coupling in the infrared. In section 6 we determine the analytic structure of the solutions in the whole momentum plane for the different types of solutions classified in section 4.3. We close with a summary and an outlook.

The results presented in sections 3.2 and 4.1 concerning the asymptotic behaviour of the equation have partly been obtained already in [2]. They have been included in some detail in the present paper since they are immediately relevant to our analysis and serve to make it self-contained.

2 The equation for the Green function of light quarks

In this section we will outline the main steps that lead to the equation for the Green function of light quarks and highlight some of its properties which are relevant to our discussion. Some of these properties and the full derivation of the equation have been discussed in detail in [2, 3].

The first step is the choice of a gauge. As noted by Gribov, the Feynman gauge turns out to be particularly well suited for deriving a simple equation which is especially sensitive to the infrared dynamics. In other gauges it would be extremely difficult to find a similarly simple equation. The physical results, like for example the occurrence of chiral symmetry breaking, will of course be independent of the choice of gauge. In Feynman gauge the gluon propagator has the form

$$D_{\mu\nu}(k) = -\frac{g_{\mu\nu}}{k^2} \alpha_s(k^2). \quad (2)$$

The exact behaviour of the strong coupling constant α_s is not known at small momenta. In Gribov's derivation of the equation it is assumed that the coupling constant is a slowly varying function of the momentum and does not become very large at small momenta. Such a behaviour is sketched in Fig. 2. It turns out that the occurrence

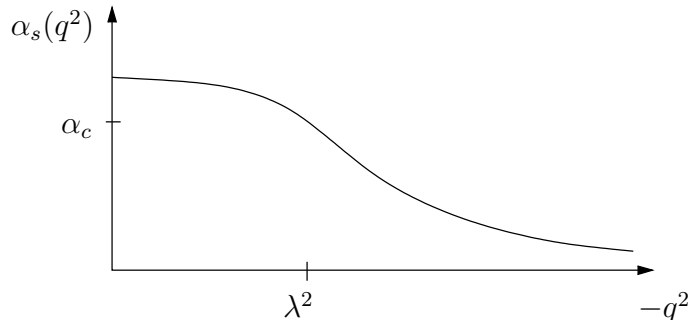


Figure 2: Assumed behaviour of the strong coupling $\alpha_s(q^2)$

of a supercritical behaviour of the Green function does not depend on the details of the coupling in the infrared, as long as its value is above the critical value in some interval of momenta. As we will see, this critical value is rather low, $\alpha_c = 0.43$. These properties of the running coupling are consistent with the picture arising in the dispersive approach [11] to power corrections in QCD (for reviews see [10, 13]). There it appears that the definition of a running coupling constant at very low momenta is possible in the sense that its integral moments have a universal meaning. Motivated by this, possible models for the coupling have been constructed, see for example [15, 16]. For our numerical study we will choose a rather simple form of the coupling, see section 4.2 below.

One starts from the Dyson–Schwinger equation for the inverse Green function G^{-1} of the quark and considers its perturbative or diagrammatic expansion. To the corresponding sum of diagrams one applies the double differentiation $\partial^2 = \partial^\mu \partial_\mu$, where ∂_μ is the derivative with respect to the external momentum q^μ of the quark. Firstly, this is a way to regularize the divergences in these diagrams, and gives a finite result. Secondly, it can be used to collect the most singular contributions to the quark Green function from the infrared region. This is based on the observation that the action of ∂^2 on the gluon propagator in Feynman gauge gives a delta function,

$$\partial^2 \frac{1}{(q - q')^2 + i\epsilon} = -4\pi^2 i \delta^{(4)}(q - q'). \quad (3)$$

The integration variables in all diagrams can be arranged in such a way that the external momentum of the quark is carried along gluon lines. If a gluon line is now differentiated twice, the above identity then transforms the integral over the corresponding gluon momentum into two zero-momentum gluon insertions. All other contributions to the respective integrals — those with derivatives in different lines or of the running coupling — are clearly less singular in the infrared region. It is in principle possible to treat these terms systematically as corrections. But the resulting equation will then be a complicated integro-differential equation, as briefly indicated in [9]. In first approximation those contributions are neglected, and one is left with a series of diagrams

with two gluon insertions that carry zero momentum. This sum can be shown to be the diagrammatic expansion of a full inverse quark Green function with two full quark–gluon vertices $\Gamma_\mu(q, k = 0)$ inserted. Using Ward identities the latter can be replaced by derivatives $\partial_\mu G^{-1}$ of the quark Green function. Having eliminated the vertex functions, one ends up with a second order differential equation for the Green function of a light quark,

$$\partial^2 G^{-1} = g(\partial^\mu G^{-1}) G (\partial_\mu G^{-1}), \quad (4)$$

where

$$g = C_F \frac{\alpha_s(q)}{\pi}. \quad (5)$$

This is Gribov’s equation which will be the subject of our study.

A comment is in order concerning the choice of scale of the running coupling in (5). As described so far, the derivation of the equation has concentrated on the most important contributions from the infrared region. But it is of course desirable to find an equation which describes the Green function correctly also in the ultraviolet region. The use of the relation (3) implies that the coupling has to be evaluated at zero momentum. But it can be shown that by replacing $\alpha_s(0)$ by $\alpha_s(q)$ one arrives at an equation that also reproduces the correct behaviour at large momenta. Given the assumptions about the running coupling discussed earlier, the correction induced by this replacement is subleading as far as its contribution to the infrared region is concerned. In the approximation presently considered we can therefore accept equation (4) with (5) as an equation that is expected to provide an adequate description of the Green function at all momentum scales.

For simplicity, equation (4) is written for one–flavour QCD. This is sufficient as long as we are mainly interested in the occurrence of confinement and chiral symmetry breaking. The generalization to the more realistic case of a doublet of light quarks is straightforward and will be important for the study of bound states in Gribov’s picture.

The fact that equation (4) is a second order differential equation implies that its solutions will involve two dimensionful constants of integration. These will be related to the quark mass and the quark condensate.

An obvious and important property of the equation is its invariance under a rescaling of the Green function, $G \rightarrow cG$ for any constant c . As a consequence, the equation will not involve the full wave function renormalization but only its logarithmic derivative. The equation is not scale invariant with respect to the momentum. The breaking of scale invariance is due to the presence of the running coupling constant. It is only through the running of the coupling that a momentum scale is introduced.

A further property of the equation is a certain symmetry between the Green function G and its inverse G^{-1} . One can easily show that the equation (4) implies

$$\partial^2 G = (2 - g)(\partial^\mu G) G^{-1} (\partial_\mu G). \quad (6)$$

This means that G solves the same equation as G^{-1} , but with g replaced by $2 - g$, the symmetry point being $g = 1$. At $g = 2$, corresponding to $\alpha_s = 3\pi/2$, the Green function would thus become a free Green function. This symmetry is certainly unphysical, and we should trust the equation only for comparatively small values of the coupling, roughly speaking below one or two. This is in agreement with the fact that in the derivation of the equation the coupling was assumed to be small.

3 Parametrization and asymptotic behaviour

3.1 Parametrization

Due to invariance under parity and Lorentz transformations the inverse Green function has the general form

$$G^{-1}(q) = a(q^2) \not{q} - b(q^2) \quad (7)$$

with two scalar functions a and b . We will in the following use the variable

$$q \equiv \sqrt{q^\mu q_\mu}, \quad (8)$$

such that the half plane $\Re q \geq 0$ already covers the full plane in q^2 , the variable in which the Green function is usually discussed. It will be convenient to use instead of (7) the following parametrization of the Green function⁴,

$$G^{-1} = -\rho \exp\left(-\frac{1}{2}\phi \frac{\not{q}}{q}\right) \quad (9)$$

with two complex functions ρ and ϕ . This corresponds to

$$a(q^2) = \frac{1}{q} \rho \sinh \frac{\phi}{2} \quad (10)$$

$$b(q^2) = \rho \cosh \frac{\phi}{2} \quad (11)$$

in the parametrization (7). The dynamical mass function M of the quark is then given by the function ϕ only,

$$M(q^2) = \frac{b(q^2)}{a(q^2)} = q \coth \frac{\phi}{2}, \quad (12)$$

whereas the function ρ represents the wave function renormalization. In terms of the usual notation we have $Z^{-1} = \rho/q$. We further introduce

$$\xi \equiv \ln q = \ln \sqrt{q^\mu q_\mu} \quad (13)$$

and denote the derivative with respect to this variable as

$$\dot{f}(q) = \partial_\xi f(q), \quad (14)$$

Since the solutions of Gribov's equation (4) depend only on the logarithmic derivative of the wave function renormalization, it is useful to define

$$p = 1 + \beta \frac{\dot{\rho}}{\rho}. \quad (15)$$

where

$$\beta = 1 - g = 1 - C_F \frac{\alpha_s}{\pi}. \quad (16)$$

Then the equation (4) for the Green function translates into a pair of coupled differential equations for p and ϕ ,

$$\dot{p} = 1 - p^2 - \beta^2 \left(\frac{1}{4} \dot{\phi}^2 + 3 \sinh^2 \frac{\phi}{2} \right) \quad (17)$$

$$\ddot{\phi} + 2p \dot{\phi} - 3 \sinh \phi = 0, \quad (18)$$

which will be the basis of our further analysis.

⁴This parametrization deviates from the one used in [3, 4].

3.2 Asymptotic behaviour

We now study the asymptotic behaviour of the solutions of Gribov's equation. An important outcome of this study will be the determination of the critical coupling at which chiral symmetry breaking occurs.

First we keep the coupling constant fixed. The running of the coupling can then be treated under the assumption that the asymptotic behaviour of the solutions depends smoothly on the coupling. This assumption will be justified by our numerical analysis further below. Since the equations (17) and (18) depend only on the logarithm of q the equations are the same along all straight lines passing through the origin of the complex q -plane. The initial conditions, at $q = 0$ for example, do not exhibit this apparent symmetry such that the solutions will be different in different directions in the q -plane. The fixed points of the equation, however, turn out to be independent of the direction in the q -plane.

Behaviour for $|q| \rightarrow \infty$

For large $|q|$ the pair of equations (17), (18) has stable fixed points at

$$\phi = (2n + 1)i\pi \quad (n \in \mathbb{Z}); \quad p = \sqrt{1 + 3\beta^2}. \quad (19)$$

As we will see in section 4.1 the existence of these fixed points implies the asymptotic freedom of the corresponding solutions.

The periodicity of the above fixed points is obvious from the equations, and we will now concentrate on the fixed point at $\phi = i\pi$. Perturbing the solutions around the fixed point,

$$\phi = i\pi + \psi; \quad p = p_0 + \hat{p} \quad (20)$$

and expanding to first order in the perturbations we find

$$p_0^2 = 1 + 3\beta^2 > 0. \quad (21)$$

Further we have

$$\partial_\xi \hat{p} = -2p_0 \hat{p}, \quad (22)$$

such that $\hat{p} = D e^{-2p_0 \xi}$ with some $D \in \mathbb{C}$. For a stable fixed point we thus have to choose the positive root $p_0 = \sqrt{1 + 3\beta^2} > 0$ in (21). We note that the function ρ consequently develops a singularity

$$\rho \sim \exp \left[\frac{p_0 - 1}{\beta} \xi \right]. \quad (23)$$

The linearized equation for ψ becomes

$$\ddot{\psi} + 2p_0 \dot{\psi} + 3\psi = 0. \quad (24)$$

Thus $\psi = C_1 e^{\gamma_+ \xi} + C_2 e^{\gamma_- \xi}$ with $C_1, C_2 \in \mathbb{C}$. We find

$$\gamma_\pm = -p_0 \pm \sqrt{3\beta^2 - 2}. \quad (25)$$

Here γ_+ and γ_- can be real ($\beta^2 > 2/3$) or complex ($\beta^2 < 2/3$). As we will see in section 5 these two possible cases have quite different physical consequences.

In the first case, $\beta^2 > 2/3$, the function ϕ approaches $i\pi$ monotonically. This case is characterized by

$$g < g_c = 1 - \sqrt{\frac{2}{3}} \simeq 0.18 \quad (26)$$

or

$$g > 1 + \sqrt{\frac{2}{3}} \simeq 1.82. \quad (27)$$

Here we find the critical value of the coupling constant α_s already mentioned earlier,

$$\alpha_c = \frac{3\pi}{4} g_c \simeq 0.43, \quad (28)$$

at which the solutions change their behaviour.

In the second case, $\beta^2 < 2/3$, the function ϕ oscillates while approaching the fixed point $i\pi$. The corresponding supercritical behaviour of the equation is characterized by values of the strong coupling constant α_s in the interval

$$\alpha_c < \alpha_s < 4.3. \quad (29)$$

The emergence of the upper limit is in agreement with the symmetry of the equation relating the Green function to its inverse for $g \rightarrow 2 - g$, see section 2. The fact that the equation exhibits subcritical behaviour at very large values of the coupling is certainly unphysical. We cannot expect that the equation describes the Green function correctly also at very large coupling.

Behaviour for $|q| \rightarrow 0$

For small $|q|$ there are two possible cases. In the first case, ϕ approaches one of the fixed points described above, $\phi = (2n + 1)i\pi$. To show this one can proceed as in the case of large $|q|$. But now we are considering $\xi \rightarrow -\infty$ and therefore have to choose the negative root in (21) in order to find a stable fixed point, $p_0 = -\sqrt{1 + 3\beta^2} < 0$. Again, the solutions will oscillate while approaching the fixed point if the coupling is supercritical.

The other case possible for $|q| \rightarrow 0$ is that ϕ vanishes at $q = 0$. Linearizing the equation for small ϕ results in

$$\ddot{\phi} + 2p_0\dot{\phi} - 3\phi = 0. \quad (30)$$

From the equation for p we find that for this fixed point $p \rightarrow p_0$ with $p_0^2 = 1$. With the ansatz $\phi = Ce^{\gamma\xi}$ it is required that $\gamma > 0$ for ϕ to be regular. In order to have a solution which at large q approaches $i\pi$ with damping we need $p_0 = 1$ and therefore $\gamma = 1$. The easiest way to see this is from eq. (34) and the corresponding discussion in section 4 below.

Running coupling

The running of the coupling can be treated assuming that the asymptotic behaviour of the solutions depends smoothly on it. The values of the function p at the fixed points discussed above depend on β . Therefore they are changed accordingly, i.e. have to be replaced by $\beta(q = 0)$ or $\beta(q = \infty) = 1$, respectively. The oscillations occurring for $|q| \rightarrow \infty$ stop at the scale at which the coupling becomes smaller than α_c , and ϕ approaches the fixed point monotonically above this scale.

4 Solutions in the Euclidean region

We first investigate the equation in the Euclidean region, i.e. for space-like momenta. Therefore we want to consider purely imaginary values of our variable q , thus $q = i\tilde{q}$ with a real-valued and positive \tilde{q} . The derivative with respect to \tilde{q} will be denoted

$$\frac{d}{d\tilde{q}}f = f'(q). \quad (31)$$

For space-like momenta the dynamical mass function $M(q^2)$ is required to be real-valued. Eq. (12) then implies that ϕ is purely imaginary. In addition, a real-valued mass function requires that the function p is real-valued for space-like momenta. For convenience we define for the use in the present section

$$\phi = i\chi, \quad (32)$$

where χ is real-valued. In this section we thus have to consider only real-valued functions χ and p depending on the real parameter \tilde{q} .

The equation (18) for χ (or ϕ , respectively) can be reformulated in such a way that it permits a simple interpretation. The function

$$\epsilon \equiv \frac{\dot{\chi}^2}{2} - 3(1 - \cos \chi) \quad (33)$$

can be interpreted as the energy of a motion with χ being a one-dimensional degree of freedom. The equation of motion equivalent to (18) is

$$\partial_\xi \epsilon = -2p\dot{\chi}^2. \quad (34)$$

The behaviour of χ can then be interpreted as a motion with damping (given by p) in the potential

$$V = -3(1 - \cos \chi). \quad (35)$$

This potential has minima at $\chi = (2n+1)\pi$ for all $n \in \mathbb{Z}$. Thus for space-like momenta the fixed points discussed in section 3.2 appear as the minima of the potential V .

4.1 Asymptotic freedom

For large $Q^2 = -q^2$ the Green function should behave according to perturbative renormalization and exhibit asymptotic freedom. We now show that Gribov's equation reproduces exactly this behaviour for solutions that approach one of the fixed points discussed above. This is done by considering the leading terms in the limit of large \tilde{q} .

We first consider the wave function renormalization. The corresponding renormalization constant is in our parametrization defined as

$$\rho = e^\xi Z^{-1}(\xi) = qZ^{-1}, \quad (36)$$

as can be seen when eq. (10) is evaluated at $\phi \simeq i\pi$. As is usually done we assume $Z(\xi)$ to be a slowly varying function. Using (15) and (17) one derives in the limit $\chi \rightarrow \pi$ the following equation⁵ for ρ ,

$$(\partial_\xi + 3)(\partial_\xi - 1)\rho + 3g\rho - g\frac{1}{\rho}(\partial_\xi \rho)^2 = 0. \quad (37)$$

⁵In [2] this equation (there eq. (4.42)) contains a misprint.

Inserting (36) and neglecting terms of the order $\partial_\xi^2 Z^{-1}$ and $(\partial_\xi Z^{-1})^2$ we find

$$\partial_\xi Z^{-1} + \frac{1}{2}gZ^{-1} = 0. \quad (38)$$

This coincides with the well-known wave function renormalization in Feynman gauge as it can be found for example in [17]. Turning to mass renormalization we observe that close to one of the fixed points, $\phi = i\chi = i(\pi - \sigma)$ with small σ , the mass function is given by (see eq. (12))

$$\sigma = 2e^{-\xi}M(\xi) = \frac{2M}{\tilde{q}}. \quad (39)$$

Linearizing eq. (18) we find

$$\ddot{\sigma} + 2\left(1 + \beta\frac{\dot{\rho}}{\rho}\right)\dot{\sigma} + 3\sigma = 0. \quad (40)$$

We further note that due to (36) and (38)

$$\frac{\dot{\rho}}{\rho} = 1 + \frac{\partial_\xi Z^{-1}}{Z^{-1}} = 1 - \frac{1}{2}g. \quad (41)$$

Together with (39) this can be inserted in (40). Neglecting the term of order $\partial_\xi^2 M$ we arrive at

$$\partial_\xi M = -\frac{3}{2}gM, \quad (42)$$

which is exactly the mass renormalization at one loop. Its solution is

$$M(q^2) = m_0 \left[\frac{\alpha_s(q^2)}{\alpha_s(q_0^2)} \right]^{\gamma_m}, \quad (43)$$

where m_0 is the mass at a given scale q_0 , and in one-loop approximation the exponent is $\gamma_m = 4/b_0$ with $b_0 = 11 - \frac{2}{3}n_f$.

Taking into account also the sub-leading solution for σ from (40) or, equivalently, from (24) we find that σ behaves at large \tilde{q} as

$$\sigma \sim \frac{2m_q}{\tilde{q}} + \frac{\nu^3}{\tilde{q}^3}, \quad (44)$$

as can be seen from (25) since in this limit $\beta \rightarrow 1$. Accordingly, the mass function behaves as

$$M(q^2) \sim m_q - \frac{\nu^3}{\tilde{q}^2}. \quad (45)$$

We thus find two dimensionful parameters, m_q and ν^3 . These can be identified with the quark mass and a quark condensate, respectively. It is difficult to disentangle the two terms in (44) numerically. We will therefore not pursue this interesting issue any further in the present paper.

4.2 Models for the running coupling

The behaviour of the strong coupling constant is only very vaguely known in the infrared region. In order to perform a numerical study we have to use a model for α_s . The model is required to be in agreement with the general assumptions used in the derivation of the equation (see section 2). Obviously, any useful model should coincide with the perturbative running of the coupling at large momentum scales. In the following we will use two different models of this kind. Both are rather simple but should be sufficient for studying the physical effects resulting from Gribov's equation. More complicated models (see for example [15, 16]) could of course be implemented in the same way.

For the perturbative behaviour of the coupling we have to specify Λ_{QCD} and n_f . Moderate changes in these parameters do not have any significant effect on our results for the Green function since they only change the behaviour of α_s at large momenta where the coupling is subcritical. To be specific we choose $\Lambda_{\text{QCD}} = 250 \text{ MeV}$ and $n_f = 3$. (The latter choice is not completely in agreement with the fact that the equation is in the present paper studied for only one flavour. The choice $n_f = 1$ would lead to almost identical results for the Green function.)

Our first model is the more realistic one, and is motivated by the dispersive approach to power corrections in QCD [11]. This approach is based on the assumption that the coupling constant can be defined down to very small momenta, and that this coupling in the infrared has a universal meaning. Then it is possible to determine its integral over the infrared region from measurements of infrared and collinear safe observables like certain event shape variables (for a recent review see [10]). In this way one finds for the integral of the coupling

$$\alpha_0 = \frac{1}{2 \text{ GeV}} \int_0^{2 \text{ GeV}} \alpha_s(k) dk \simeq 0.5. \quad (46)$$

This condition can be fulfilled by shifting the argument of the logarithm in the usual one-loop formula for the perturbative running of the coupling,

$$\alpha_s(q^2) = \frac{4\pi}{\left(11 - \frac{2}{3}n_f\right) \ln(-q^2/\Lambda_{\text{QCD}}^2 + a)}. \quad (47)$$

For $a = 0$ this is exactly the one-loop renormalization of the coupling. Our first model for the running coupling is obtained for $a = 6$. This choice is made to satisfy the condition (46). We will in the following refer to this model as type A. This running of the coupling is shown as curve A in Fig. 3. For comparison we show in that figure as curve C also the coupling obtained from the one-loop renormalization.

The second model is shown as curve B in Fig. 3. It is obtained from the one-loop renormalization of the coupling (see eq. (47) with $a = 0$) by simply cutting it off at some given value and assuming it to be constant below the corresponding momentum scale. In order to avoid problems in the numerical treatment of the equation we smooth out the resulting edge by fitting a polynomial of third degree such that the first derivative is continuous. Apart from this detail the coupling in this model, which we will refer to as type B, is uniquely determined by a given value $\alpha_s(0)$ at vanishing momentum. This model is in general, i. e. for arbitrary $\alpha_s(0)$, not in agreement with the condition (46). It is not constructed to serve as a realistic description of the strong coupling. Instead,

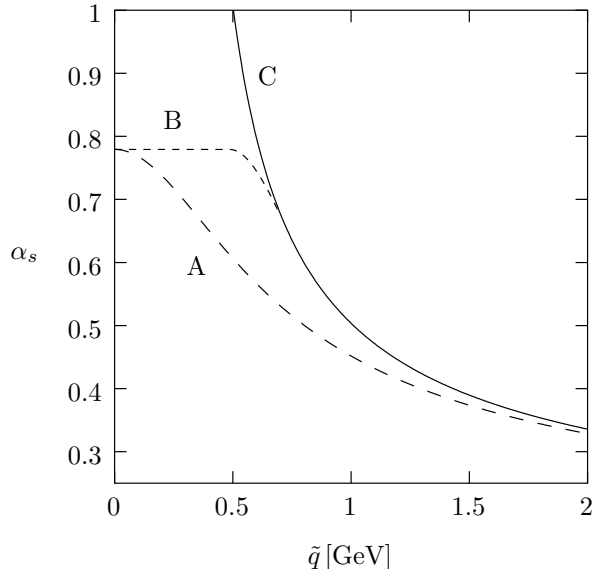


Figure 3: Models for the strong coupling constant (A, B) and the behaviour according to one-loop renormalization (C)

it will mainly be used in order to study the qualitative effects of Gribov's equation. For this purpose a model is useful in which the coupling is clearly supercritical in a large region of momenta. It will also be useful to vary the strength of the coupling and to study the effects resulting from this change. Similarly, a comparison between the results obtained with coupling of type A and of type B will be interesting. The differences will in that case also depend on the initial conditions of the solutions.

4.3 The solutions in the Euclidean region

We now turn to the numerical study of the pair of differential equations (17), (18) in the Euclidean region of space-like momenta. We have used two different numerical methods. All solutions presented below have been found using a Runge-Kutta procedure, i.e. the step-wise integration of the equation starting from a set of given initial conditions. We have also used the routine COLSYS [18], a non-local collocation procedure using B-splines which is also suited for boundary-value problems with boundary conditions given at different points. Within numerical errors agreement has been found in all cases in which both methods have been applied.

The solutions in the Euclidean region can be classified according to their behaviour at small and large momenta \tilde{q} . As discussed in section 3.2, the possible fixed points for $\tilde{q} \rightarrow 0$ and $\tilde{q} \rightarrow \infty$ differ from each other by the values of the function χ (or equivalently ϕ). The values of p are then fixed in the respective limits. Due to the 2π -periodicity of the equations in χ we can restrict ourselves in the following to the case in which $\chi \rightarrow \pi$ for $\tilde{q} \rightarrow \infty$. We will distinguish three classes of solutions in which the function χ approaches in the limit $\tilde{q} \rightarrow 0$ the values 0 (or 2π), $-\pi$, or π , respectively. We will now discuss these three classes separately.

The solutions in the first class⁶ start at $\chi(\tilde{q} = 0) = 0$. As discussed in section 3.2 this implies $p(0) = 1$. The free parameter in this class of solutions is therefore $\chi'(0)$ (or, equivalently, the renormalized mass m_R , see section 5 below). Here and in the following we will measure \tilde{q} in units of GeV, and thus χ' in units of GeV^{-1} . For small $\chi'(0)$ the function χ approaches π monotonically. Such a solution is shown in Fig. 4, and we have plotted both χ and p . If the coupling constant is subcritical for all \tilde{q}

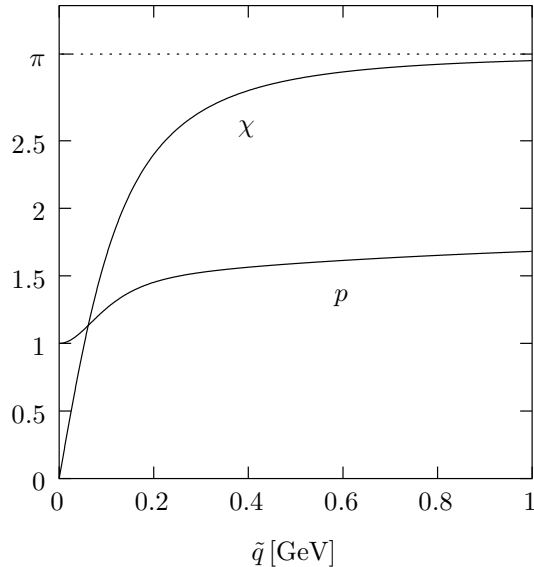


Figure 4: Solutions χ and p for $\chi'(0)=20$ (corresponding to $m_R=100$ MeV, see below) with running coupling of type A

(for example for model B with $\alpha_s(0) < \alpha_c$) the solution is monotonic for all possible $\chi'(0)$. This situation changes if the coupling constant is supercritical in some interval of momenta. For small values of $\chi'(0)$ the solution is still monotonic, c.f. the solution in Fig. 4 which is found for supercritical coupling. Due to the smallness of $\chi'(0)$ these solutions come close to π only at momentum scales at which the running coupling is already subcritical again, and we do not observe oscillations. But for larger values of $\chi'(0)$ the function χ increases more rapidly and can pass the value π . Such a solution is shown in Fig. 5. For even larger $\chi'(0)$ the function χ can pass π more often, and in fact even arbitrarily often for $\chi'(0) \rightarrow \infty$. However, these oscillations are very strongly damped as the scale on the vertical axis in Fig. 5 illustrates. In all cases the solutions stop oscillating as \tilde{q} increases. This was to be expected since the coupling becomes subcritical at larger momentum scales. If $\chi'(0)$ is negative the function χ approaches $-\pi$ instead of π at large \tilde{q} . Due to the periodicity of the equations in χ we can then assume that these solutions start at $\chi(0) = 2\pi$ (instead of 0) and approach the fixed point π . Otherwise the behaviour of these solutions (oscillations, damping etc.) is not different from the case of positive $\chi'(0)$.

In the second class of solutions χ runs from $-\pi$ to π as \tilde{q} runs from 0 to ∞ . In other words, χ goes from one minimum of the potential to a neighboring one. At the same

⁶These are the (only) solutions discussed in [2].

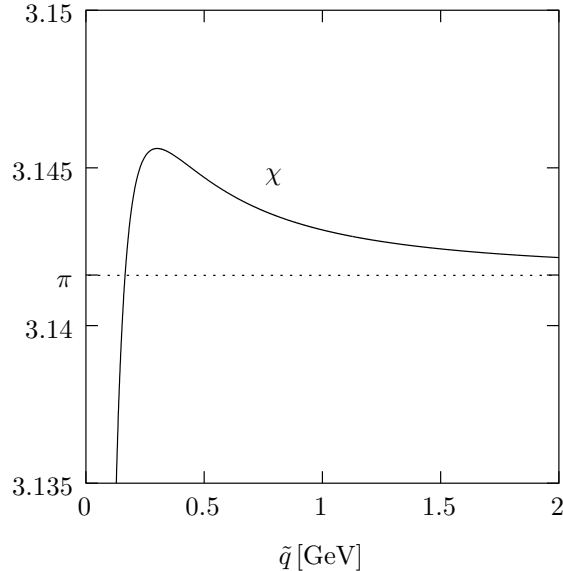


Figure 5: Solution χ for $\chi'(0) = 250$ (corresponding to $m_R = 8$ MeV, see below) with running coupling of type A

time p runs from $-\sqrt{1 + 3\beta^2(0)}$ to $\sqrt{1 + 3\beta^2(\infty)} = 2$. It is possible that the zeros of χ and p coincide. Such a solution is presented in Fig. 6. In a sense, these solutions are ‘symmetric’. (This term would be more appropriate if the coupling was not running but constant.) There are also solutions in which the zeros of χ and p do not coincide, they are ‘asymmetric’ in this sense.

The third class comprises such solutions in which χ starts at π and also approaches this value at large \tilde{q} . The solutions thus stay in one well of the potential. At the same time p runs over the same range as in the previous class of solutions. Similar to that case, it is possible that $\chi = \pi$ and $p = 0$ coincide. Such a ‘symmetric’ solution is shown in Fig. 7. Of course, there are also ‘asymmetric’ solutions in which these special values of χ and p occur at different momentum scales.

If the coupling is supercritical the solutions of the second and third class can exhibit oscillations of χ around π (and also around $-\pi$ for $\tilde{q} \rightarrow 0$ in the third class) similar to the ones described above for the first class.

Numerically, the solution of the first class can be found by integrating the equation starting at $\tilde{q} = 0$. In order to integrate the solutions numerically for the second and third class one has to start at some intermediate \tilde{q}_0 . This is no restriction since the matching of two solutions for $0 < \tilde{q} < \tilde{q}_0$ and $\tilde{q}_0 < \tilde{q} < \infty$ is trivial. It just reflects the fact that integrating a differential equation starting from a stable fixed point leads to exponentially large numerical errors.

The three classes discussed above exhaust all asymptotically free solution in the Euclidean region, i. e. solutions which end up in one of the fixed points for $\tilde{q} \rightarrow \infty$. Especially, there are no solutions in which χ runs from a minimum of the potential (35) to any other minimum that is not a neighboring one.

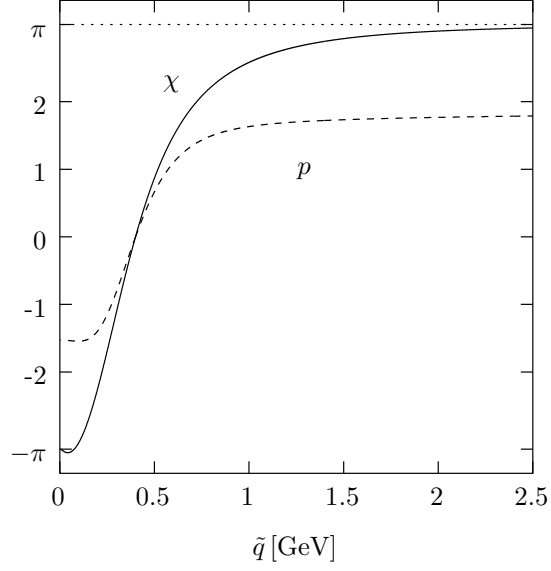


Figure 6: Solutions χ and p for $\chi(0.4) = 0$, $\chi'(0.4) = 10$ and $p(0.4) = 0$ with running coupling of type A

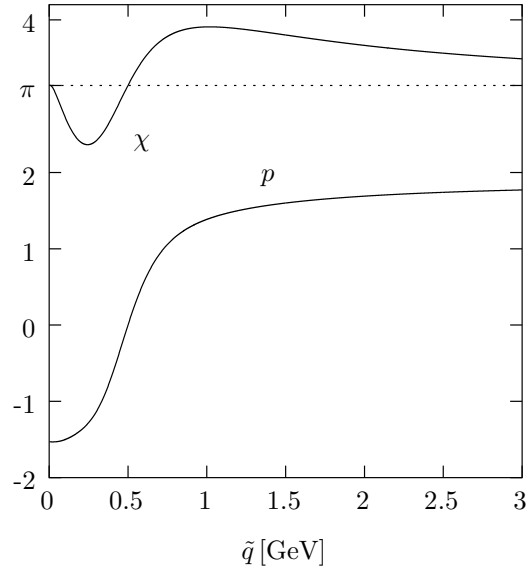


Figure 7: Solutions χ and p for $\chi(0.5) = \pi$, $\chi'(0.5) = 4$ and $p(0.5) = 0$ with running coupling of type A

5 Mass renormalization and chiral symmetry breaking

In this section we would like to address the question how the dynamical mass function $M(q^2)$ of the quark behaves in the Euclidean region for the solutions discussed in the preceding section. We will mainly concentrate on the first class of solutions and only briefly comment on the other two classes at the end of the section.

Let us define⁷ the ‘renormalized’ mass m_R as the limit of the mass function $M(q^2)$ as the momentum vanishes,

$$m_R = \lim_{\tilde{q} \rightarrow 0} M(q^2). \quad (48)$$

Since in the first class of solutions $\chi(0) = 0$ we can expand (12) to find that the renormalized mass becomes

$$m_R = \frac{2}{\chi'(0)}. \quad (49)$$

Since $\chi'(0)$ was just the free parameter specifying these solutions we can use m_R instead to characterize them uniquely. Although the renormalized mass is the small-momentum limit of the dynamical mass function it would most probably be too simple to interpret it as a constituent mass of the quark.

Further we want to define a ‘perturbative’ mass m_P of a given solution. It is supposed to reflect the behaviour of the perturbative tail of the mass function of this solution. This could be achieved by computing its asymptotic behaviour which is eventually described by eq. (43). For our purposes it turns out to be sufficient and more convenient for the numerical study to choose a definition which involves only a finite momentum scale. We therefore define the perturbative mass as the value of the mass function at the scale λ at which the coupling becomes subcritical (see also Fig. 2) and the perturbative behaviour is expected to set in,

$$m_P = M(\lambda^2) = \lambda \cot \frac{\chi(\lambda)}{2}. \quad (50)$$

Obviously, the scale λ in this definition depends on the model for the running coupling. In the models A and B discussed in section 4.2, and presumably in most other realistic models, the values of λ are very similar. Any other choice of scale would lead to similar results as long as that scale is chosen larger than λ .

A general property of the solutions of Gribov’s equation is the rapid decrease of the mass function with increasing momentum. This is illustrated in Fig. 8 for two solutions that are similar to the one shown in Fig. 4. Both solutions in this figure do not exhibit oscillations since they correspond to comparatively small values of $\chi'(0)$ (see also the corresponding discussion in section 4.3).

It is now interesting to study the relation between the renormalized mass m_R and the perturbative mass m_P . First we consider the case of subcritical coupling. We choose model B for the running coupling with a maximal value $\alpha_s(0) = 0.3$. Since the coupling is subcritical for all momenta the scale λ cannot be defined via the critical value α_c in this model. Therefore we have to supplement the definition (50) of the

⁷This term was introduced in [2] and we adopt it here. This mass is not meant to be renormalized as opposed to being a bare mass in the usual sense. The mass function of course describes the mass renormalization for all q^2 . This ‘renormalization’ is done down to $\tilde{q} = 0$, having in mind a starting point at large \tilde{q} .

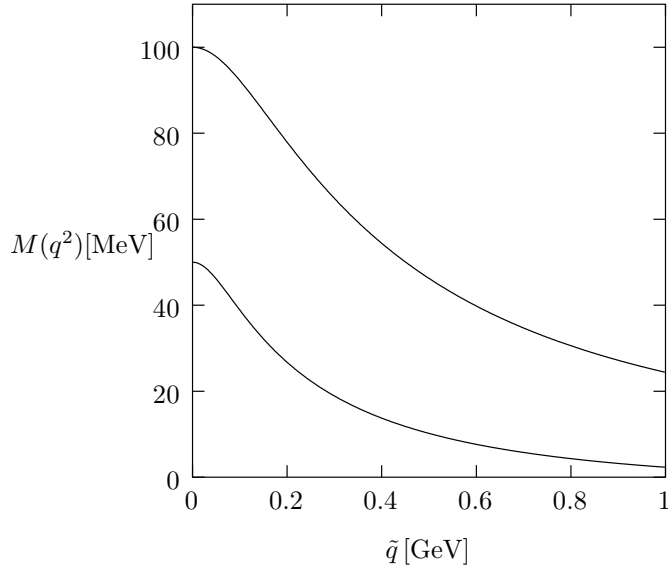


Figure 8: The mass function $M(q^2)$ for renormalized masses $m_R = 50$ MeV and 100 MeV, respectively, for coupling of type A

perturbative mass with the choice $\lambda = 1$ GeV in this case. This choice is to some extent arbitrary. It is mainly motivated by the values of λ resulting from the models A or B with supercritical $\alpha_s(0)$. Other choices for λ in the subcritical case lead to similar results for the dependence of m_R on m_P . This dependence is shown in Fig. 9. For subcritical coupling there is a one-to-one correspondence between renormalized mass m_R and perturbative mass m_P . The renormalized mass decreases with decreasing perturbative mass, and vanishes when the perturbative mass vanishes. Chiral symmetry is thus not broken at subcritical coupling.

If the coupling is supercritical at small momenta some of the solutions exhibit oscillations. These are possible until the running coupling becomes subcritical, i.e. as long as $\tilde{q} < \lambda$. There are also monotonic solutions for which m_R has to be sufficiently large (see section 4.3). Let us consider one of the latter. The corresponding function χ has a certain value at the scale λ . But there are also solutions χ with smaller $m_R = 2/\chi'(0)$ which oscillate and pass π twice. It is now possible that one of these solutions has the same value at the scale λ as the monotonic solution considered before. There can in fact be even more solutions with this property, among them also solutions with negative m_R (resp. negative $\chi'(0)$). The number of these solutions will (for $m_P \neq 0$, see below) remain finite. The reason for this is the following. A solution χ which oscillates very often will be very close to π due to the strong damping in the corresponding equation. As a result there is a maximal possible $\chi(\lambda)$ which the solutions can reach for a given number of oscillations. In summary, we find that different values of m_R (resp. $\chi'(0)$) can lead to identical values of $\chi(\lambda)$. But since the perturbative mass m_P depends only on this value $\chi(\lambda)$, see (50), the correspondence between the renormalized and the perturbative mass is no longer one-to-one. Instead it takes the form shown in Fig. 10, and the renormalized mass becomes a multi-valued function of the perturbative mass. Here we have chosen model B for the running coupling, thus $\lambda = 1.27$ GeV. Further

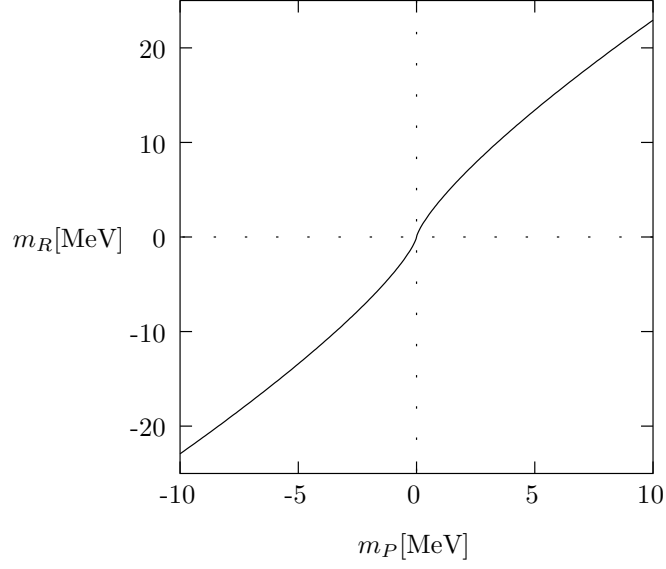


Figure 9: Renormalized mass m_R vs. perturbative mass m_P for subcritical coupling (coupling of type B with $\alpha_s(0)=0.3$)

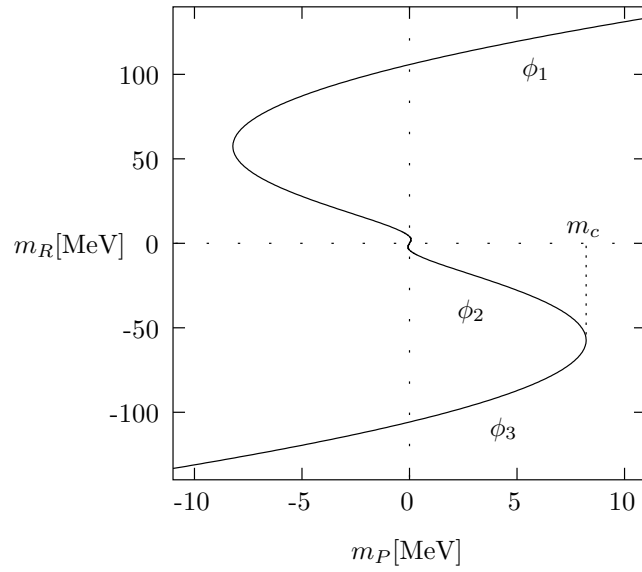


Figure 10: Renormalized mass m_R vs. perturbative mass m_P for coupling of type B with $\alpha_s(0)=0.94$

we have chosen $\alpha_s(0) = 0.94$ in this figure because the effect is more pronounced at large coupling. The dependence on the coupling strength and on the model will be studied below. The figure has been obtained by integrating the differential equation up to $\tilde{q} = \lambda$ with varying initial conditions $\chi'(0)$.

Fig. 10 shows that at supercritical coupling the renormalized mass does not vanish in the limit of vanishing perturbative mass, and we thus find that chiral symmetry is broken. This figure is one of our main results and we will now study it in some more detail. At large perturbative mass there is only one branch of solutions, denoted as ϕ_1 in the figure. But if the perturbative mass is below a critical mass m_c there are two additional solutions with different renormalized mass, denoted as the branches ϕ_2, ϕ_3 in the figure, and we can regard this as a phase transition in the vacuum of light quarks. If we consider only the region of positive perturbative masses we can identify the branch ϕ_1 with monotonic solutions, whereas the branch ϕ_3 corresponds to solutions in which χ passes π . Further, the branch ϕ_2 can be identified with solutions in which χ passes π and in addition has a turning point.

We observe that the curve in Fig. 10 is symmetric with respect to the origin. This is an immediate consequence of the fact that the equations (17), (18) are invariant under the exchange

$$\phi \rightarrow 2\pi i - \phi. \quad (51)$$

The mass function changes sign under this transformation, and hence the symmetry.

The phase transition at the critical value m_c of the perturbative mass m_P is not the only one. In fact there is an infinite series of similar phase transitions taking place in the limit $m_P \rightarrow 0$. The curve in Fig. 10 exhibits a very interesting self-similarity which illustrates this series of phase transitions. In Fig. 11 we show a detail of Fig. 10 around the origin. Both figures show different parts of the same curve. We denote

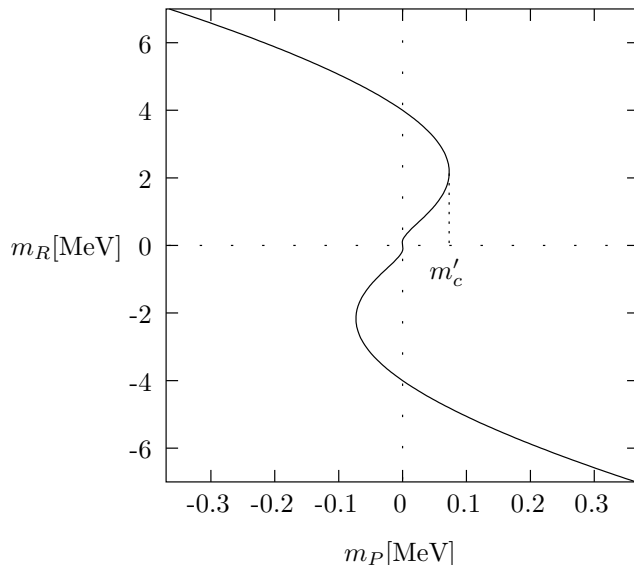


Figure 11: Renormalized mass m_R vs. perturbative mass m_P for coupling of type B with $\alpha_s(0)=0.94$, detail of Fig. 10

the critical mass of the second phase transition as m'_c . In the two additional solutions

occurring at this scale the function χ passes the value π twice.

It is interesting to note that in each phase transition one of the two additional branches of solutions has the quite unusual property that the renormalized mass grows with decreasing perturbative mass.

The phase transitions lead to the generation of pions as Goldstone bosons [2, 3]. The Bethe–Salpeter amplitude of the pion can be shown to be $\varphi = C\{G^{-1}, \gamma_5\}$ with a constant C . It solves an equation for $q\bar{q}$ bound states which is derived in a similar approximation scheme as the equation for the Green function [2]. It has been speculated that the observation of just one pion in nature should restrict the physical value of the perturbative mass of the quark to be between the first and second phase transition [19]. As can already be seen from Figures 10 and 11, however, two successive phase transitions happen to take place at mass scales which differ from each other by two orders of magnitude. Therefore it is not possible to deduce any considerable restriction on the physical perturbative mass of the quark in this way.

It is now instructive to study the dependence of the critical mass scales on the value and on the model chosen for the running coupling. For this we use the two models A and B for the running coupling introduced in section 4.2. There we did not yet define how to vary the coupling strength in model A. We will use the value $\alpha_s(0)$ at vanishing momentum as a parameter (as in model B) and adjust the value of a in eq. (47) accordingly to obtain a running coupling of varying strength in this model as well. Of course, the condition (46) will then no longer be fulfilled. In model B the momentum scale λ at which the coupling becomes critical is independent of the value $\alpha_s(0)$, but in model A it depends by construction on the parameter a . Since this dependence is rather weak and in order to make the results comparable we use also for model A the fixed value $\lambda = 1.27 \text{ GeV}$ which is obtained for model B.

Fig. 12 shows the dependence of the first critical mass m_c on the coupling strength in models A and B. In order to obtain this figure we have computed curves similar to the one in Fig. 10 for different values of the coupling and determined the turning point corresponding to m_c . Below the critical coupling there are no phase transitions and the critical mass acquires values different from zero only for supercritical values of the coupling. As expected, the critical mass then grows with increasing coupling. Realistic values of the coupling are roughly of the order $\alpha_s(0) \simeq 0.8$ (model A), corresponding to $g(0) \simeq 0.3$. From Fig. 12 we see that in this region both models give very similar values for the critical mass m_c in the range of a few MeV. Only for perturbative quark masses below this small m_c we expect chiral symmetry breaking. This is in perfect agreement with Gribov’s physical picture according to which exactly the existence of very light quarks with masses below of few MeV leads to a dramatic change in the vacuum structure.

At very large values of the coupling there is a maximum and the critical mass decreases again. For model B this maximum is reached at $g(0) \simeq 1.1$, and for model A it is found at $g(0) \simeq 1.5$ (outside the range shown in Fig. 12). This seemingly strange behaviour has its origin in a property of the equation that we noticed already in sections 3.2. There we found that the oscillations in the solutions χ around the value π disappear at very large coupling $g > 1 + \sqrt{2/3}$. Had we chosen a fixed value for α_s instead of a running α_s in Fig. 12 we would have found in fact that the critical mass vanishes again at $g = 1 + \sqrt{2/3}$. But in our models the running coupling is a continuous function. Even for arbitrarily large $g(0)$ it has in some momentum range values which

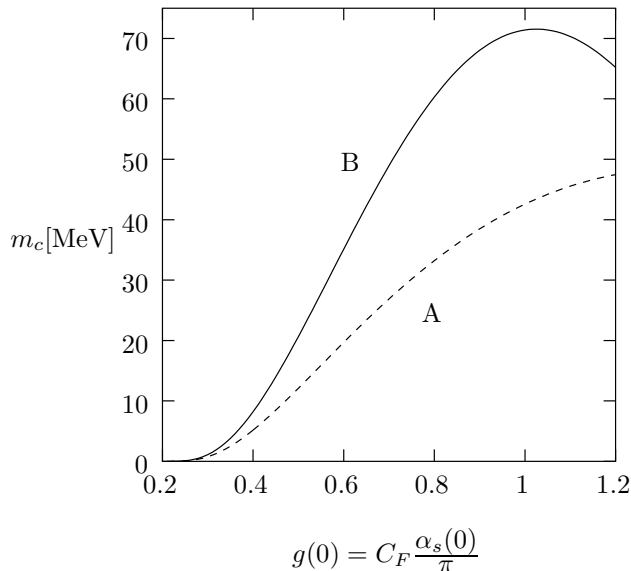


Figure 12: Critical mass m_c of the first phase transition as a function of the coupling with behaviour of type A and B, respectively

make oscillations possible, and m_c does not vanish even at large coupling. Obviously, this is true for all possible continuous shapes of the running coupling. We therefore expect that the occurrence of chiral symmetry breaking due to this mechanism is largely independent of the details of the running coupling at small momenta.

In Fig. 13 we show the second critical mass m'_c as a function of the coupling. As we already mentioned the values of m'_c are almost two orders of magnitude smaller than the corresponding values of the first critical mass m_c . The behaviour of m'_c at very large coupling (not shown in the figure) is analogous to the behaviour observed for the first critical mass, and there is a similar maximum and decrease at very large $g(0)$.

Finally, we would like to comment on the solutions of the second and third class found in section 4.3. Here the interpretation in terms of a renormalized mass is more involved than in the solutions of the first class discussed above. This is because here we find $\chi(0) = -\pi$ (second class) or $\chi(0) = \pi$ (third class), respectively. According to (12) this implies that a renormalized mass defined as the limit of the mass function at zero momentum, see (48), would always vanish. Nevertheless, it should be possible to define a quantity similar to the renormalized mass m_R at some intermediate but small momentum scale. In the second and third class of solutions the behaviour at large momenta is similar to that of the first class, especially concerning the oscillations. Given a suitable definition of a renormalized mass in the above sense one would therefore observe similar phase transitions and the breaking of chiral symmetry. A full interpretation of the renormalized mass, especially for the second and third class of solutions, remains to be found. Most probably this would require a better understanding of the difficult problem of the emergence of a constituent mass of the quark.

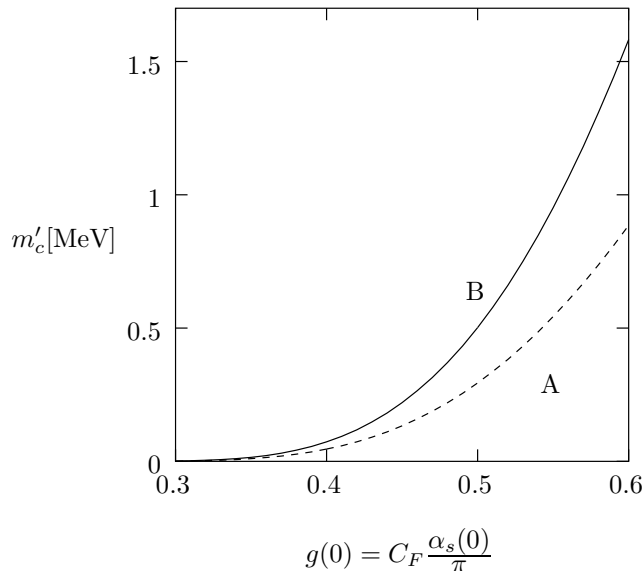


Figure 13: Critical mass m'_c of the second phase transition as a function of the coupling with behaviour of type A and B, respectively

6 Analytic structure of the solutions

So far we have discussed the properties of the solutions of Gribov's equation in the region of space-like momenta. Now we turn to the problem of determining the corresponding analytic structure of the Green function in the whole momentum plane. The locations and nature of the singularities in the complex q^2 plane contain crucial information about the solutions, especially about their properties regarding causality and confinement. It has been argued in [4] that a suitable solution for the retarded Green function of a confined quark should be free of singularities in the physical region $\Im m q^2 \geq 0$. The analysis of the first class of solutions (see section 4.3) in [3] has shown that we should not expect to find such a confining solution of the equation without pion corrections. We will confirm that result and extend it also to the two other classes of solutions.

As a first step we need to define the coupling constant in the whole complex momentum plane. This problem, however, is poorly understood even at large momenta since the one-loop formula for the running coupling does not possess a unique analytic continuation. Obviously, the situation is even worse at low $|q|$. In order to avoid additional parameters and artificial singularities we will therefore make the simplest possible assumption and choose a fixed coupling throughout the complex q -plane. The value of this coupling will be chosen to be supercritical, and in the examples below $\alpha_s = 0.8$. We have to hope that this choice will be a suitable approximation at least for small $|q|$. For large $|q|$ our choice seems less appropriate. But it will turn out that the singularities of the Green function occur at comparatively small values of $|q|$, probably indicating that an adiabatic modification of the coupling at large $|q|$ would not change the analytic structure. Obviously, the choice of a constant and supercritical coupling disagrees with the models for α_s we have used to find the solutions in the Euclidean region. The details of the solutions will in fact change at large space-like momenta.

But we have checked that the classification of the solutions given in section 4.3 remains valid.

In order to study the analytic structure we integrate the equation along suitable contours in the complex plane. These should start in the Euclidean region where the necessary conditions on the initial values are known and the possible solutions have been classified (see section 4.3). Some typical contours are shown in Fig. 14. In general

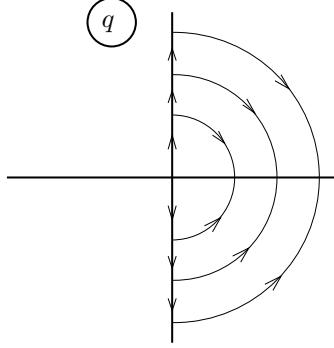


Figure 14: Typical contours in the q -plane

(especially for the solutions of the second and third class) the contours need not start in the origin of the q -plane. We should remind the reader that our definition (8) implies that the right-hand half of the q -plane already covers the full q^2 -plane, and the Euclidean region is given by the vertical axis in Fig. 14.

The occurrence of poles and cuts in the analytic continuation will in general lead to a complicated Riemann surface. We will in the following only discuss singularities arising in the physical region of the q -plane, although it is in principle possible to locate also further singularities on unphysical sheets of the Riemann surface.

We start with the solutions of the first class for which $\phi(q=0) = 0$ and $\phi \rightarrow i\pi$ for large space-like q , see Fig. 4 for a typical example. The different solutions of this class are parametrized by the renormalized mass m_R . All of these solutions have a pole on the real (time-like) q -axis and a cut along this axis starting at the pole. There are no other singularities in the physical region of the q -plane⁸. This result holds for all solutions of this class independent of their renormalized mass. In particular, this structure is found even for solutions which are located on different branches in Fig. 10. The singularity and the cut on the real axis have been discussed in [2, 3] but there the absence of further singularities could not be proved. To illustrate our result we show in Fig. 15 the continuation of the solution of Fig. 4, i. e. in this solution again $m_R = 100 \text{ MeV}$. In this and in the following figures the momentum q is given in units of GeV. The cut is clearly visible. Below the cut the function ϕ is real-valued on the real axis. The starting point of the cut coincides with a pole of the Green function at $q = m^*$, and in our example $m^* = 128 \text{ MeV}$. The pole is most easily seen in the function p , the real part of which is plotted in Fig. 16 in a small region around the pole. At this point the function ρ (see eq. (9)) vanishes such that the Green function develops a pole. In general, the pole on the real axis moves to larger values of m^* when

⁸There are further poles on the unphysical sheets of the cut which we will not discuss here.

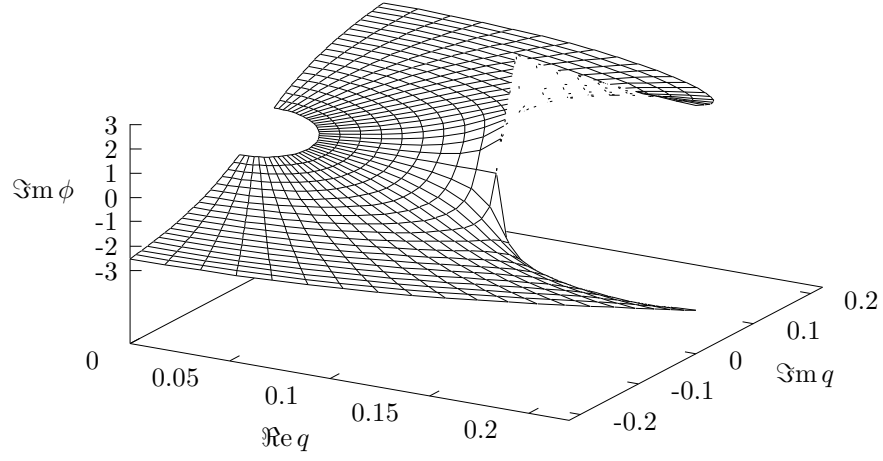


Figure 15: Continuation of $\Im m \phi$ of the solution in Fig. 4 with a cut on the real q -axis

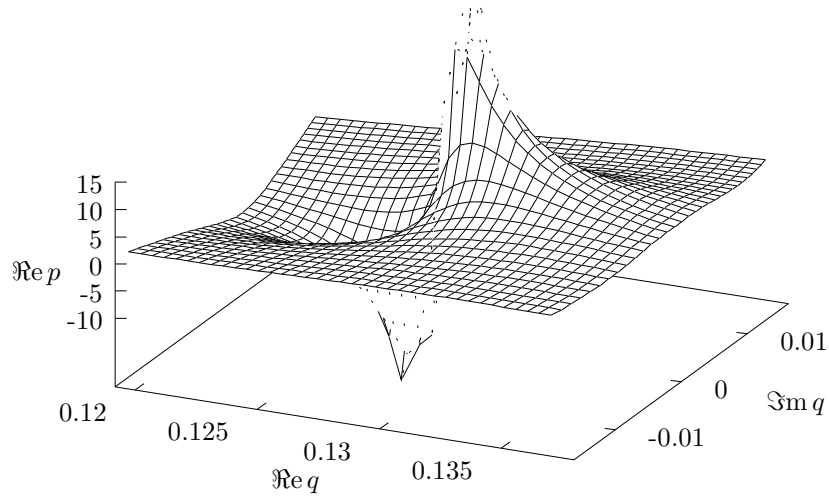


Figure 16: Pole of $\Re p$ on the real axis, continuation of the solution in Fig. 4

m_R is increased.

This analytic structure of the Green function in the first class of solutions resembles the analytic structure in perturbation theory. The position of the pole can be interpreted as the mass m^* of a propagating particle. Obviously, these solutions do not lead to confined quarks.

Let us now consider the solutions of the second class in which ϕ runs from $-i\pi$ to $i\pi$ in the Euclidean region. These solutions have been obtained in section 4.3 by choosing at some point $q_A = ir$ on the imaginary q -axis the initial values $\phi = 0$ and $p = 0$. (This is the ‘symmetric’ case, for the other case see below.) We find that in all solutions of this kind the Green function develops a pole exactly on the circle with radius r , with a cut starting at the pole. The exact position of the pole depends on the value chosen for $\chi'(q_A)$. (In this section we give this parameter of the solutions in terms of χ rather than in terms of ϕ since $\chi'(q_A)$ is real-valued and in order to make it easier to compare with the preceding section. We recall that the functions are related by $\phi = i\chi$ and the derivative is with respect to $\tilde{q} = -iq$, see eq. (31).) For small values of this parameter the pole is close to the real q -axis, and can in fact be shifted arbitrarily close to the real axis by choosing sufficiently small $\chi'(q_A)$. For larger values of this parameter the pole moves along the circle towards the imaginary q -axis. In all cases the pole is found in the physical region above the real axis. In addition, there are two further poles and cuts in the physical region. These two poles are located under the same polar angle in the q -plane. For smaller values of $\chi'(q_A)$ they are located closer to the real axis, and the one located at smaller $|q|$ moves closer to the origin, whereas the other one moves to larger distances from the origin. At all three poles the function ρ vanishes. As an example we show in Fig. 17 the function $\Im m \phi$ for the same solution which is shown in Fig. 6 in the Euclidean region, i. e. for the solution obtained from $r = 0.4 \text{ GeV}$ and $\chi'(q_A) = 10$. The shape of the cuts in the figure is due to the choice of the contours of

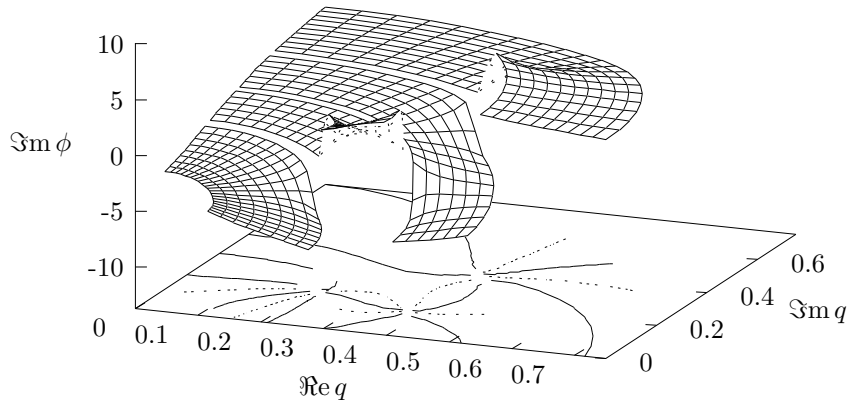


Figure 17: $\Im m \phi$ in the physical region, continuation of the solution in Fig. 6

integration. The corresponding poles can be found again by looking at the function p . Their positions can be seen in Fig. 6 as the points where the contour lines meet. There are further singularities in the unphysical region which we do not discuss here.

There are further solutions in the second class which we called ‘asymmetric’ in section 4.3 in which the zeros of ϕ and p in the Euclidean region do not coincide. Also

these solutions have a singularity in the physical region on the circle on which $p = 0$ is chosen on the imaginary q -axis. As in the ‘symmetric’ solution this pole can be shifted very close to the real axis but not below it. The ‘asymmetric’ solutions also have further singularities but we will not discuss them here.

Finally, there is the third class of solutions in which ϕ stays close to $i\pi$ throughout the Euclidean region. Here the situation is similar to the one for the solutions of the second class. We find a pole and a cut on the circle on which on the imaginary q -axis $p = 0$. Again this is the case for the ‘symmetric’ solutions (in which $p = 0$ coincides with $\phi = i\pi$ on the imaginary axis) as well as for the ‘asymmetric’ solutions. As an example we present in Fig. 18 the analytic structure of the ‘symmetric’ solution that we have shown in Fig. 7. The crosses and lines correspond to the poles and cuts. The solid line indicates on which sheets of the cut the other singularities are located. Denoting

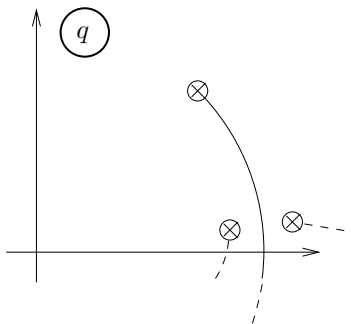


Figure 18: Positions of the singularities in the physical region of the q -plane for the continuation of the solution in Fig. 7

again as q_A the point on the imaginary axis at which $\phi = 0$ and $p = 0$, we have for this solution $q_A = i \cdot 0.5 \text{ GeV}$ and $\chi'(q_A) = 4$. For smaller values of $\chi'(q_A)$ the pole moves towards the real axis but stays in the physical region. There are two further poles and cuts as indicated in the figure. These two poles are located on a straight line that goes through the origin.

In summary, we have found in this section that the analytic structure of the solutions of the first class is similar to the analytic structure of a perturbative Green function. For this class we find a pole and a cut on the real q -axis and no other singularities in the physical region. In the other two classes there are poles and cuts on the physical sheet. Those solutions will in general not permit an interpretation in agreement with causality and unitarity and should therefore be regarded as unphysical solutions of Gribov’s equation. We did not find any hint for the existence of exceptional solutions in which those singularities move to the unphysical sheet for special initial conditions. We can thus conclude that, as anticipated in [3], there are no solutions of the equation without pion corrections which would lead to confined quarks.

7 Summary and outlook

The subject of this paper has been Gribov’s equation for the Green function of light quarks. We have have outlined how this equation is derived from the Dyson–Schwinger

equation, and we have described how the approximations made in the derivation are motivated by the physical picture of supercritical color charges in QCD. In Gribov's scenario the phenomenon of supercritical charges can occur in QCD due to the existence of very light quarks and is expected to cause chiral symmetry breaking and confinement. In the present paper we have concentrated on the equation proposed in [2, 3] which does not yet contain pion corrections. The equation describes the Green function in Feynman gauge. It collects the most singular contributions to the Dyson–Schwinger equation coming from the region of small momenta. At the same time it reproduces asymptotic freedom at large momenta. The derivation of the equation involves the assumption that the running coupling remains finite at small momentum scales. This is in agreement with recent phenomenological results obtained in the dispersive approach to power corrections in QCD. These analyses find a typical value of the coupling in the infrared which is above the critical value $\alpha_c = 0.43$ arising in Gribov's scenario.

Gribov's differential equation for the light quark's Green function is a nonlinear equation and so far only asymptotic expansions had been used to study it. We have described the corresponding results, especially the fixed point structure of the equation resulting from this analysis and the emergence of the critical value of the strong coupling. We have then performed a complete numerical study of the equation. After defining suitable models for the behaviour of the strong coupling constant in the infrared region we have classified the possible solutions of the equation according to their behaviour in the Euclidean region of space-like momenta. At supercritical coupling the solutions change their behaviour and can oscillate while approaching the fixed points. The dynamical mass function of the quark has been computed in order to show that this change leads to the breaking of chiral symmetry at supercritical coupling. Chiral symmetry breaking takes place independently of the details of the running coupling in the infrared as long as it is supercritical in some interval of the momentum. The breaking of chiral symmetry is connected with the occurrence of a series of phase transitions in the vacuum of light quarks. If the perturbative mass m_P of the quark, i. e. the mass defined at a large momentum scale, is below a critical mass then there are several solutions leading to different quark masses m_R at low momentum scales, and in general m_R does not vanish even in the limit of vanishing perturbative mass m_P . We have determined the critical mass as a function of the coupling. It turns out to depend considerably on the mean value of the coupling in the infrared, but the dependence is weaker if the coupling is only slightly above the critical value. In agreement with the physical picture of supercritical color charges the phase transitions occur only for very small values of the perturbative quark mass.

In [3, 4] it has been advocated that a confining Green function in Gribov's picture should be free of singularities in the physical region including time-like momenta. We have therefore studied the solutions of Gribov's equation in the whole complex momentum plane. One class of solutions has an analytic structure similar to that of a perturbative Green function, whereas the other two classes of solutions have singularities on the physical sheet. As anticipated in [3] there are no solutions of the equation studied in the present paper exhibiting the structure required for confinement.

The phase transitions connected with the breaking of chiral symmetry lead to the generation of pions as Goldstone bosons. Their special properties in this approach [3] indicate that they should be taken into account as elementary objects, and that the equation for the Green function of the light quark should be modified accordingly. This

modification [4] is expected to change the behaviour of the solutions in the Euclidean region only very little. In particular, the breaking of chiral symmetry will take place in a very similar way. But the pion corrections to the equation are expected to have significant effects on the analytic structure of the solutions. Due to that it appears possible to find a confining Green function. The next step should therefore be a numerical study of the corresponding differential equation. Although the modified equation with pion corrections is more complicated it can be analysed using the same methods that have been used in the present paper. It would at a later stage also be interesting to investigate the effects of an additional scalar (σ -)meson which has been widely discussed in the literature in the context of meson spectra and of sigma models.

We hope that the results of our analysis will be useful also for the more conventional approach to the Dyson–Schwinger equation for the quark. Some general properties of the Green function resulting from the Dyson–Schwinger equation appear to be rather universal and largely independent of the particular approximation scheme that is used. The analysis of the Dyson–Schwinger equation in quenched supercritical QED [20], for example, leads to a picture of phase transitions and chiral symmetry breaking that is very similar to the one resulting from Gribov’s equation. It would certainly be useful to identify such universal features of the Green function and to achieve a better understanding of their origin. In this respect it is very important to consider different approximation schemes among which Gribov’s approach is certainly exceptional since it is motivated by the very interesting physical picture of supercritical charges.

Acknowledgements

This work would not have been possible without numerous very instructive and motivating discussions with the late Vladimir Gribov. It is very sad that he passed away much too early. I missed his advice very much during the later stages of this work.

I am most grateful to Yuri Dokshitzer for many very helpful discussions and for a careful reading of the manuscript, and to Christian Gawron for invaluable advice. I would like to thank Bernard Metsch, Julia Nyiri, Herbert Petry, Dieter Schütte, Manfred Stingl, Bryan Webber, and Anthony Williams for helpful discussions. I am grateful to the Institut für Theoretische Kernphysik of the University of Bonn where part of this work was carried out. Finally, I would like to thank the CERN Theory Division for hospitality extended to me during the final stages of this work.

References

- [1] V. N. Gribov, *Physica Scripta* **T 15** (1987) 164
- [2] V. N. Gribov, *Possible Solution of the Problem of Quark Confinement*, Lund preprint LU-TP 91-7 (1991)
- [3] V. N. Gribov, *Eur. Phys. J. C* **10** (1999) 71 [hep-ph/9807224]
- [4] V. N. Gribov, *Eur. Phys. J. C* **10** (1999) 91 [hep-ph/9902279]
- [5] W. Greiner, B. Müller, J. Rafelski, *Quantum Electrodynamics of Strong Fields*, Springer, Berlin, 1985

- [6] V. N. Gribov, Orsay lectures on confinement (I - III):
LPT Orsay 92-60, hep-ph/9403218;
LPT Orsay 94-20, hep-ph/9404332;
LPT Orsay 99-37, hep-ph/9905285
- [7] V. N. Gribov, in Proceedings of the International School of Subnuclear Physics, 34th Course, Erice, Italy, 1996, ed. A. Zichichi, World Scientific, p. 30
- [8] F. E. Close, Yu. L. Dokshitzer, V. N. Gribov, V. A. Khoze, M. G. Ryskin, *Phys. Lett. B* **319** (1993) 291
- [9] Yu. L. Dokshitzer, in Proceedings of the International School of Subnuclear Physics, 31th Course, Erice, Italy, 1993, ed. A. Zichichi, World Scientific, p. 108
- [10] Yu. L. Dokshitzer, in Proceedings of 29th International Conference on High Energy Physics (ICHEP 98), Vancouver, Canada, 1998, p. 305 [hep-ph/9812252], and references therein
- [11] Yu. L. Dokshitzer, G. Marchesini, B. R. Webber, *Nucl. Phys. B* **469** (1996) 93 [hep-ph/9512336]
- [12] Yu. L. Dokshitzer, B. R. Webber, *Phys. Lett. B* **352** (1995) 451 [hep-ph/9504219];
Phys. Lett. B **404** (1997) 321 [hep-ph/9704298];
M. Beneke, V. M. Braun, V. I. Zakharov, *Phys. Rev. Lett.* **73** (1994) 3058;
M. Beneke, V. M. Braun, *Phys. Lett. B* **348** (1995) 513 [hep-ph/9411229];
P. Ball, M. Beneke, V. M. Braun, *Nucl. Phys. B* **452** (1995) 563 [hep-ph/9502300];
R. Akhoury, V. I. Zakharov, *Phys. Lett. B* **357** (1995) 646 [hep-ph/9504248];
Nucl. Phys. B **465** (1996) 295 [hep-ph/9507253];
G. P. Korchemsky, G. Sterman, *Nucl. Phys. B* **437** (1995) 415 [hep-ph/9411211];
in Proc. 30th Recontres de Moriond, Meribel les Allues, France, 1995, J. Tran Thanh Van (ed.) (Editions Frontiers, 1995) [hep-ph/9505391]
- [13] M. Beneke, *Phys. Rep.* **317** (1999) 1 [hep-ph/9807443]
- [14] C. D. Roberts, A. G. Williams, *Prog. Part. Nucl. Phys.* **33** (1994) 477 [hep-ph/9403224]
- [15] B. R. Webber, *J. High Energy Phys.* **10** (1998) 012 [hep-ph/9805484], and references therein
- [16] D. V. Shirkov and I. L. Solovtsov, *Phys. Rev. Lett.* **79** (1997) 1209 [hep-ph/9704333]
- [17] A. J. Buras, *Rev. Mod. Phys.* **52** (1980) 199
- [18] U. Ascher, J. Christiansen, R. D. Russell, *Math. Comp.* **33** (1979) 659
- [19] S. D. Bass, *Phys. Lett. B* **329** (1994) 358 [hep-ph/9404294]
- [20] F. T. Hawes, T. Sizer, A. G. Williams, *Phys. Rev. D* **55** (1997) 3866 [hep-ph/9608292]